Shape Reconstruction From Photometric Stereo

Kyoung Mu Lee and C.-C. Jay Kuo
Signal and Image Processing Institute
Department of Electrical Engineering-Systems
University of Southern California
Los Angeles, California 90089-2564

Abstract

Two new iterative algorithms for shape reconstruction based on multiple images taken under different lighting conditions known as photometric stereo are proposed. It is shown in this research that single-image SFS algorithms have an inherent problem, i.e. the accuracy of the reconstructed surface height is related to the slope of the reflectance map function defined on the gradient space. This observation motivates us to generalize the single-image SFS algorithm to two photometric stereo SFS algorithms aiming at more accurate surface reconstruction. The two algorithms directly determine the surface height by minimizing a quadratic cost functional, which is defined to be the squares of the brightness error obtained from each individual image in a parallel or cascade manner. The optimal illumination condition which leads to best shape reconstruction is also examined.

1 Introduction

Extracting the surface information of an object from its shaded image, known as the shape from shading (SFS) problem, is one of the fundamental problems in computer vision. Many SFS algorithms using a single image have been developed [1], [2], [3], [6], [8]. However, it is well known that this problem is ill-posed so that the solution may not be reliable. Thus, researchers have also considered the use of multiple images to provide additional information for robust surface reconstruction, which includes the photometric stereo method [4], [10], [11] and the geometric stereo method [5], [9].

The photometric stereo method was first proposed by Woodham [10], [11]. With this method, one uses images taken from the same viewing direction under different lighting conditions. The surface orientation of a local point is determined by its irradiances in these images by using the fact the orientation corresponds to the intersection of constant brightness contours of different reflectance maps on the gradient space. Since it is a local method where the surface orientation is determined point by point, it is applicable without the smooth surface and the constant albedo constraints. However, integrability problem arises in this method and it is sensitive to noise.

In this research, we first show that the single-image SFS algorithm may not yield an accurate result by examining the characteristics of the reflectance map, and explain how to use the photometric stereo information to improve the accuracy of the reconstructed surface. We propose two robust SFS algorithms which determine the surface height directly using photometric stereo images and call them the parallel and cascade schemes. The optimal illumination condition which leads to best shape reconstruction is also discussed in the current setting and verified experimentally.

2 Single-Image SFS

The basic equation for the image formation process can be expressed by the *image irradiance equation*

$$E(x,y) = R(p,q), \tag{1}$$

where R is called the reflectance map function. The reflectance map can be derived that

$$R(p,q) = \begin{cases} \eta \mathbf{l}^T \mathbf{n}, & \mathbf{l}^T \mathbf{n} \geq 0, \\ 0, & \mathbf{l}^T \mathbf{n} < 0, \end{cases} \tag{2}$$

where η is the albedo of the surface,

$$\mathbf{n} = \frac{(-p,-q,1)^T}{\sqrt{1+p^2+q^2}}$$

is the surface normal, and

$$\mathbf{l} = \frac{(-p_s,-q_s,1)^T}{\sqrt{1+p_s^2+q_s^2}} = (\cos\tau\sin\sigma, \sin\tau\sin\sigma, \cos\sigma)^T$$

is the unit vector of the illumination direction pointing toward the light source, and where τ and σ are the

0-8186-2855-3/92 $3.00 ©1992 IEEE

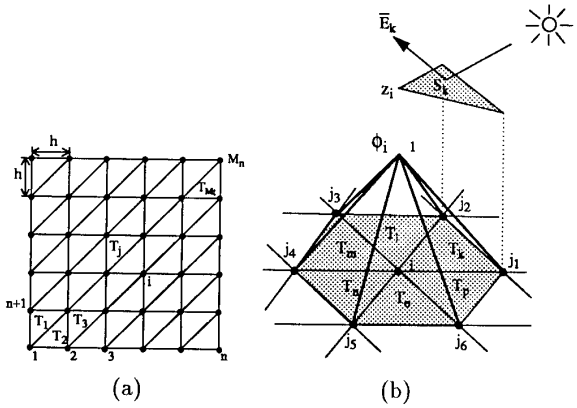

Figure 1: (a) A uniform triangulation of a square domain Ω; (b) A nodal basis function ϕ_i.

tilt and *slant* angles and p_s and q_s denote the slope of a surface element perpendicular to the illumination direction.

Consider the approximation of a smooth surface with a union of triangular surface patches over a uniform grid domain as illustrated in Fig. 1(a). The approximating surface can be expressed as a linear combination of basis functions ϕ_i with local compact support known as the finite triangular elements (see Fig. 1(b)) such that

$$z(x,y) = \sum_{i=1}^{M_n} z_i \phi_i(x,y),$$

where z_i is the value of $z(x,y)$ at the ith node and M_n is the number of nodal basis functions. Then, the orientation of a triangular patch can be determined as

$$p(x,y) = \sum_{i=1}^{M_n} z_i \frac{\partial \phi_i(x,y)}{\partial x}, \quad q(x,y) = \sum_{i=1}^{M_n} z_i \frac{\partial \phi_i(x,y)}{\partial y}. \tag{3}$$

Combining finite triangular surface model with the linearized reflectance map image formation model, we can express the image irradiance directly in terms of nodal heights of triangular elements as follows.

$$E = R(p,q) \approx \alpha p + \beta q + \gamma = \sum_{i=1}^{M_n} \Phi_i z_i + \gamma, \tag{4}$$

where

$$\begin{aligned} \Phi_i(x,y) &= \alpha \frac{\partial \phi_i(x,y)}{\partial x} + \beta \frac{\partial \phi_i(x,y)}{\partial y}, \\ \gamma &= R(p_0,q_0) - \alpha p_0 - \beta q_0, \end{aligned}$$

and

$$\alpha = \frac{\partial R(p,q)}{\partial p}\Big|_{(p_0,q_0)}, \quad \beta = \frac{\partial R(p,q)}{\partial q}\Big|_{(p_0,q_0)}.$$

To estimate the nodal heights z_i, we consider the cost functional which involves brightness error and regularization term,

$$\mathcal{E} = \iint_\Omega (E_o - E)^2 \, dx\, dy + \frac{\lambda}{2} \iint (z_{xx}^2 + 2z_{xy}^2 + z_{yy}^2) \, dx\, dy, \tag{5}$$

where E_o and E denote the observed and generated image irradiance by the reflectance map model, and λ is the smoothing factor. By substituting (4) into (5) and discretize the second term, we obtain

$$\begin{aligned} \mathcal{E}_b &= \iint_\Omega [E_o - (\sum_{i=1}^{M_n} \Phi_i z_i + \gamma)]^2 \, dx\, dy + \frac{1}{2} \mathbf{z}^T \mathbf{B} \mathbf{z} \\ &= \frac{1}{2} \mathbf{z}^T \mathbf{C} \mathbf{z} - \mathbf{b}^T \mathbf{z} + c, \quad \mathbf{C} = \mathbf{A} + \lambda \mathbf{B}, \end{aligned} \tag{6}$$

It can be shown [6] that although the *stiffness* matrix $\mathbf{A}$ and the *smoothness* matrix $\mathbf{B}$ are symmetric positive semi-definite, $\mathbf{C}$ is usually symmetric positive definite. Then the minimization problem is equivalent to the solution of the linear system of equations

$$\mathbf{C}\mathbf{z} = \mathbf{b}.$$

Efficient iterative linear system solvers such as multigrid method or PCG (Preconditioned Conjugate Gradient) method can be applied for its solution.

To obtain more accurate reconstructed surface, a successive linearization scheme is applied to the reflectance map. That is, we linearize the reflectance map with respect to the local gradient point of the triangular patch obtained from the previous iteration, and perform the above solution procedure repeatedly.

3 Characteristics of the Reflectance Map

Since the SFS algorithm is an inverse process which recovers the surface orientations from the image irradiance through the reflectance map, the characteristics of the reflectance map play an important role in this problem. For simplicity, let us fix the value of $q = q_0$ and view the reflectance map $R(p,q_0)$ as a function of one variable p. The corresponding irradiance equation becomes

$$E = R(p,q_0). \tag{7}$$

The sensitivity of p with respect to the change in E can be estimated via

$$\left|\frac{\Delta p}{\Delta E}\right| = \left|\left(\frac{\partial R(p,q_0)}{\partial p}\right)^{-1}\right|, \tag{8}$$

which is inversely proportional to the slope of the reflectance map at point p. Thus, for a fixed value of ΔE, the estimate $\hat{p}$ is more accurate (i.e. smaller value of Δp) for the region where $R(p, q_0)$ is steeper. Similar arguments can be made along the q-direction.

The contour plots of two typical reflectance maps are given in Figs. 2(a) and (b). They are skewed along the line passing through $(0,0)$ and (p_s, q_s). If the spacings between the adjacent contour lines are narrower (or wider), the slopes of the reflectance map $R(p,q)$ are steeper (or smoother), or equivalently, the partial derivatives $R_p(p,q)$ and $R_q(p,q)$ of the reflectance map have larger (or smaller) absolute values. For a given point (p_0, q_0) in the gradient space, the sensitivity is highest along the gradient direction, i.e.

$$\nabla R(p_0, q_0) = (R_p(p_0, q_0), R_q(p_0, q_0)),$$

and lowest along the tangential direction, i.e. $(-R_q(p_0, q_0), R_p(p_0, q_0))$.

In practice, real images contain noises such as the sensor, quantization and modeling error noises. Since the image is corrupted by these noises, it is relatively difficult to obtain accurate surface orientations or heights in the region where the slope of the reflectance map is smooth [7]. Moreover, note that the components of the stiffness matrix $\mathbf{A}$ are determined primarily by the partial derivatives of the reflectance map with respect to p and q [6]. Therefore either small values of the partial derivatives $R_p(p,q)$ or $R_q(p,q)$ cause some elements of the stiffness matrix to be nearly zero and make the problem ill-conditioned so that the height or orientation related to those elements cannot be easily determined. We observe that smaller values of the partial derivatives $R_p(p,q)$ and $R_q(p,q)$ often slow down the convergence rate of the iterative algorithm. The slow convergence behavior is clearly attributed to the large condition number of the original nonlinear minimization problem (5).

4 Two Photometric Stereo SFS Algorithms

The photometric stereo images provide several reflectance map functions, which can be used to enhance the sensitivity of Δp and Δq with respect to ΔE over the gradient domain of our interest.

Given J different photometric stereo images E_{oj} with their corresponding reflectance maps $R_j(p,q)$, $j = 1, \ldots, J$, we consider two different schemes to combine them, namely, the parallel and cascade schemes. The parallel scheme is to use all images at the same time, and formulate all $R_j(p,q)$, $1 \le j \le J$, in one cost functional,

$$\mathcal{E} = \iint \sum_{j=1}^{J} (E_{oj} - E_j)^2 \, dx \, dy + \frac{\lambda}{2} \iint (z_{xx}^2 + 2z_{xy}^2 + z_{yy}^2) \, dx \, dy, \tag{9}$$

where E_{oj} and E_j are the jth observed and parameterized images, respectively. By using the triangular element surface model and the linearized reflectance model, we can express (9) in the discrete form,

$$\mathcal{E} = \frac{1}{2}\mathbf{z}^T \tilde{\mathbf{C}} \mathbf{z} - \tilde{\mathbf{b}}^T \mathbf{z} + c, \quad \tilde{\mathbf{C}} = \tilde{\mathbf{A}} + \lambda \mathbf{B}, \tag{10}$$

where the overall stiffness matrix $\tilde{\mathbf{A}}$ and the load vector $\tilde{\mathbf{b}}$ are the sum of each individual stiffness matrix $\mathbf{A}_j$ and the load vector $\mathbf{b}_j$, i.e.

$$\tilde{\mathbf{A}} = \sum_{j=1}^{J} \mathbf{A}_j, \qquad \tilde{\mathbf{b}} = \sum_{j=1}^{J} \mathbf{b}_j. \tag{11}$$

The nodal height vector $\mathbf{z}$ is the vector which minimizes the quadratic functional (10) and can be obtained by solving the linear system of equations,

$$\tilde{\mathbf{C}} \mathbf{z} = \tilde{\mathbf{b}}. \tag{12}$$

In contrast, the cascade scheme uses the photometric stereo images one after another in a cascade manner. The single-image SFS algorithm is used for each image and the previous result is used as the initial condition.

5 The Optimal lighting Conditions

To improve the performance of the single-image SFS algorithm, we incorporate reflectance maps that compensate each other's weakness. We know from Section 2 that

$$p_s = -\frac{\cos\tau \sin\sigma}{\cos\sigma},$$

and

$$q_s = -\frac{\sin\tau \sin\sigma}{\cos\sigma}.$$

Thus, the angle θ which the line passing through $(0,0)$ and (p_s, q_s) makes with the p-axis and the distance d between $(0,0)$ and (p_s, q_s) can be written as

$$\theta = \arctan\left(\frac{q_s}{p_s}\right) = \arctan(\tan\tau) = \tau,$$

$$d = \sqrt{p_s^2 + q_s^2} = \tan\sigma,$$

Table 1: The rms error of the reconstructed surface heights according to the variation of tilt angle of the second image for the parallel and the cascade schemes, (tilt, slant) = (45°, 45°) are fixed for the first image and slant = 45° are fixed for the second image.

tilt(°)	parallel	cascade
0	0.125186	0.187297
15	0.128692	0.231566
30	0.192990	0.360646
45	0.447816	0.431678
60	0.181018	0.336983
75	0.109999	0.218857
90	0.093384	0.208685
105	0.087438	0.226707
120	0.085450	0.221273
135	0.076186	0.237868
150	0.079959	0.225893
165	0.084040	0.210219
180	0.132937	0.186983
195	0.170376	0.201333
210	0.170710	0.261275
225	0.168250	0.347342
240	0.149476	0.299825
255	0.121514	0.217509
270	0.090110	0.192800
285	0.085979	0.204031
300	0.096235	0.210975
315	0.078121	0.214341
330	0.080660	0.212522
345	0.099063	0.214217

respectively. Note that the angle θ is exactly the same as the tilt angle τ, and the distance d depends only on the slant angle σ. Therefore, the tilt angle determines the orientation of the reflectance map around the origin whereas the slant angle determines the distance between the origin and (p_s, q_s) in the gradient space as well as the shape of the reflectance map. The angle between the two gradient directions of the reflectance maps with tilt angles τ_1 and τ_2 is simply $|\ \tau_1 - \tau_2\ |$.

If the slant angle is in the range between 30° and 60°, the reflectance map covers the central region of the gradient space which is our main concern and has appropriate values in steepness. Thus, the optimal lighting condition is primarily dependent on the tilt angles of different light sources and not sensitive to the slant angles as long as they are between 30° and 60°. We know from the discussion in Section 3 that the reflectance map provides good sensitivity along the gradient direction but poor sensitively along the tangential direction. Consider two photometric stereo images illuminated from the same slant angle but different tilt angles. It is ideal that the gradient directions of one reflectance map correspond to the tangential directions of the other reflectance map over the region of our interest. This can be achieved by choosing the difference of their tilt angles to be 90°, One such example is given by Fig. 2(c), where the contour plots of two reflectance maps are shown together. Note that the gradients of a smooth surface are usually concentrated on the central region of the gradient space, say, $-0.5 < p, q < 0.5$. It is clear from these two figures that the gradient direction of one reflectance map is the tangential direction of the other and vice versa in this region. To summarize, the optimal lightening condition can be written as

$$|\ \tau_1 - \tau_2\ | = 90°. \tag{13}$$

The condition (13) can be verified by the experimental results shown in Table 1. The test object is the sombrero surface shown in Fig. 3(a). We see from these data that the parallel scheme produces more accurate reconstructed surface and the best result is obtained when the tilt angles of the two photometric stereo images are orthogonal to each other. That is, when the tilt angle of the second image is around 135° or 315° in this example. The error becomes larger when the two images are illuminated from similar tilt angles.

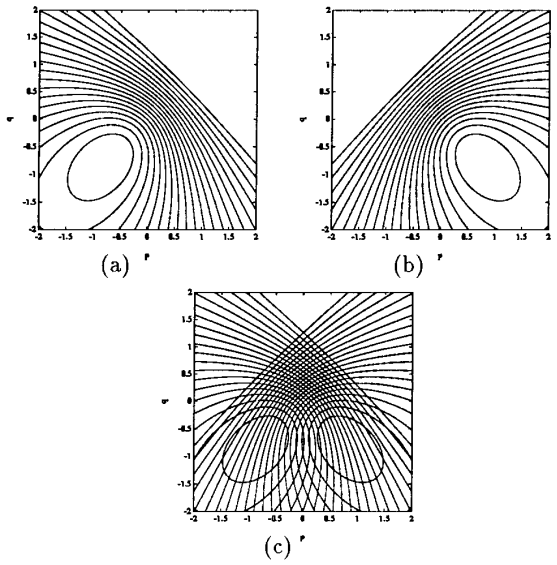

Figure 2: Contour plots of two reflectance maps with (a) (albedo, tilt, slant) = (250, 45°, 45°) or $(p_s, q_s) = (-0.707, -0.707)$; (b) (albedo, tilt, slant) = (250, 135°, 45°) or $(p_s, q_s) = (0.707, -0.707)$; (c) combined reflectance map of (a) and (b).

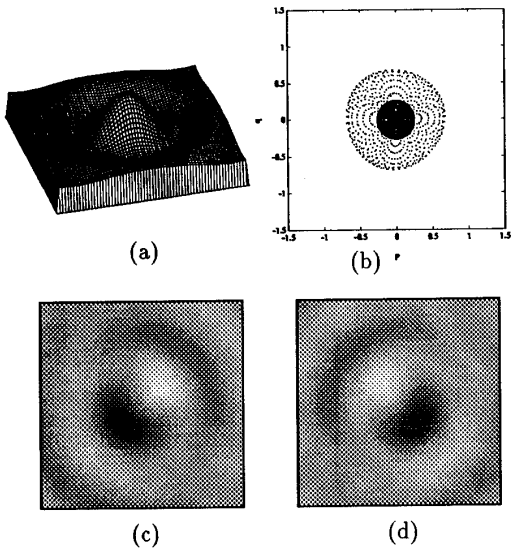

Figure 3: The sombrero test problem: (a) 3-D height plot, (b) (p, q) distribution in the gradient space, (c) synthesized image with (albedo, tilt, slant) = $(250, 45°, 45°)$, (d) synthesized image with (albedo, tilt, slant) = $(250, 135°, 45°)$.

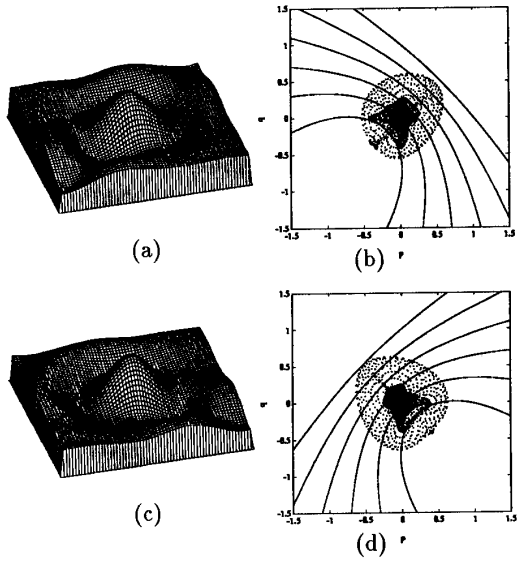

Figure 4: Results of the single-image SFS algorithm applied to the sombrero image: (a) and (b) the reconstructed height, the corresponding (p, q) plot from the image of Fig. 3(c), (c) and(d) the reconstructed height, the corresponding (p, q) plot from the image of Fig. 3(d).

6 Experimental Results

Test Problem 1: Sombrero

The tested photometric stereo images are shown in Figs. 3 (c) and (d) which are generated from the sombrero surface as shown in Fig. 3(a). Note that these two images are shaded by light sources with orthogonal tilt angles. The (p, q) distribution of the true sombrero surface is given in Fig. 3(b).

Results of the single-image SFS algorithm applied to Figs. 3(c) and (d) are given in Fig. 4. The results are not good in some regions. By comparing the distribution of these (p, q) values with the original one, we see clearly that points move very slowly along the tangential directions of the contours. The results of the parallel and cascade schemes are shown in Fig. 5. By comparing the (p, q) distribution of the parallel scheme and the single-image method to the original one, we see that a significant improvement has been achieved by using the parallel scheme. This is due to that the two reflectance maps help each other and provide good sensitivity over the interested region of the gradient space as discussed in Sections 3 and 5. The cascade scheme provides a better result over the single-image SFS algorithm. However, it performs slightly worse than the parallel scheme as shown in Table 1.

Test Problem 2: Agrippa

The test images are 128 x 128 real images of the Agrippa statue as shown in Figs. 6(a) and (b). The results of the single-image SFS algorithm, the parallel and cascade schemes are shown in Figs. 6(c)-(f). We observe from Figs. 6(c) and (d) that ambiguities occur for both surfaces in several regions including cheeks. Moreover, the shadow problem is quite serious. It is evident from Figs. 6(e) and (f) that a great deal of improvement has been achieved by parallel and cascade scheme. We conclude that more accurate results are produced by using the photometric stereo schemes, in particular, by using the parallel scheme.

7 Conclusion

We have shown that the accuracy of the reconstructed surface and the performance of the single-image SFS algorithm are highly related to the slop of the reflectance map function in the gradient space. Based on this observation, we proposed two new iterative SFS algorithms, i.e. parallel and cascade schemes, using multiple photometric stereo images taken under different lighting conditions.

Experimental results show that both schemes produce more accurate reconstructed surface compared to the single-image SFS algorithm. The effect of dif-

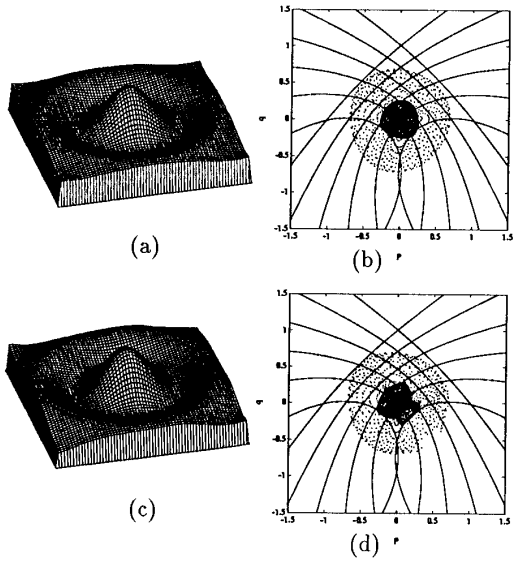

Figure 5: Results of the photometric stereo SFS algorithms applied to the sombrero image: (a) and (b) the reconstructed height, the corresponding (p, q) plot by the parallel scheme, (c) and (d) the reconstructed height, the corresponding (p, q) plot by the cascade scheme.

ferent illumination directions of two light sources is also tested. We conclude that the best result can be obtained when the two illumination directions are orthogonal to each other, since their reflectance maps complement each other in the optimal way in the central region of the (p, q) domain.

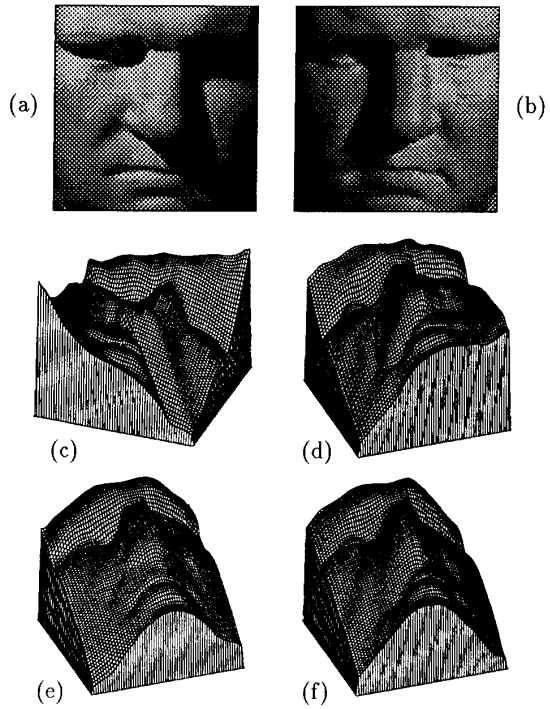

Figure 6: The Agrippa test problem: two real images of the Agrippa statue illuminated with (a) (tilt, slant) = $(135°, 50°)$; (b) (tilt, slant) = $(45°, 45°)$; (c) and (d) are the reconstructed heights from (a) and (b) by the single-image SFS algorithm; (e) and (f) are the reconstructed heights by the photometric stereo SFS algorithms with the parallel and cascade schemes, respectively.

References

[1] R. T. Frankot and R. Chellappa, "A method for enforcing integrability in shape from shading algorithm," *IEEE Trans. Pattern Anal. Machine Intell.*, Vol. 10, No. 4, pp. 439–451, 1989.

[2] B. K. P. Horn, "Height and gradient from shading," *International Journal of Computer Vision*, Vol. 5, pp. 584–595, 1990.

[3] B. K. P. Horn and M. J. Brooks, "The variational approach to shape from shading," *Computer Vision, Graphics, and Image Processing*, Vol. 33, pp. 174–208, 1986.

[4] K. Ikeuchi, "Determining surface orientations of specular surfaces by using the photometric stereo Method," *IEEE Trans. Pattern Analysis and Machine Inteligence*, Vol. PAMI-13, No. 6, pp. 661–669, 1981.

[5] K. Ikeuchi, "Reconstructing a Depth Map from Intensity Maps," in *IEEE Conference on Computer Vision and Pattern Recognition*, (Canada), pp. 736–738, July 1984.

[6] K. M. Lee and C.-C. J. Kuo, "Shape from shading with a linear trinagular element surface model," Tech. Rep. 172, USC, Signal and Image Processing Institute, 1991. Also to appear in *IEEE Trans. Pattern Analysis and Machine Inteligence.*

[7] K. M. Lee and C.-C. J. Kuo, "Shape reconstruction from photometric stereo," Tech. Rep. 197, USC, Signal and Image Processing Institute, 1992. Submitted to the *Journal of Optical Society of America: A.*

[8] A. P. Pentland, "Shape information from shading: a theory about human perception," in *Proc. of International Cof. on Computer Vision*, pp. 404–413, 1988.

[9] M. Shao, R. Chellappa, and T. Simchony, "Reconstructing a 3-D depth map from one or more images," *Computer Vision, Graphics, Image Processing: Image Understanding*, Vol. 53, pp. 219–226, March 1991.

[10] R. J. Woodham, "Photometric method for determining surface orientation from multiple images," *Optical Engineering*, Vol. 19, No. 1, pp. 139–144, 1980.

[11] R. J. Woodham, "Analysing images of curved surfaces," *Artificial Intelligence*, Vol. 17, No. 1-3, pp. 117–140, 1981.